Aperture-Averaging - Theory and Measurements

N. Perlot, D. Fritzsche
German Aerospace Center (DLR), D-82234 Wessling, Germany

ABSTRACT

Atmospheric laser communications using direct-detection systems do suffer from severe degradation caused by scintillation. Because the atmospheric cut-off frequency can be as low as 100 Hz, temporal averaging is not applicable in high-speed communications. The simplest way of reducing fading is to increase the receiver size and to take advantage of aperture averaging. Spatial and temporal variations of the received intensity have to be investigated in order to predict the efficiency of aperture averaging.

This paper reviews briefly the theory of spatial averaging that characterizes the direct-detected optical power. For comparison purposes, results of measurements are presented. These measurements consist of recorded pupil intensity patterns for a scenario with known turbulence profile. Statistics derived from measurement data are compared with theoretical second-order statistics.

keywords: aperture averaging, scintillation, atmospheric turbulence, frozen turbulence hypothesis

1. INTRODUCTION

1.1. Paper outline

A direct detection receiver collects the irradiance flux over its aperture and focuses it on a detector. In this way, the collecting aperture acts as a spatial filter of the irradiance in the receiver plane and reduces the received signal fluctuations that arise from scintillation.

In this paper, we first recall some theoretical background on second-order statistics of the irradiance flux process. Subsequently, discussions are made about various irradiance flux statistics extracted from a sequence of intensity images that have been recorded on a CCD camera. The chosen experimental scenario presented in this paper is a 2.9 km near-ground scenario that is suited for CCD measurements.

In section 2 the experimental setup is described. The measurement method is assessed by highlighting its advantages and its weaknesses. Focusing on the experimental scenario, the PDF of the irradiance flux is evaluated and commented in section 3. In section 4, the application of the frozen turbulence hypothesis is discussed. This hypothesis states that the turbulent cells are in movement primarily because of the wind transverse to the direction of propagation. In order to evaluate the validity of the space-domain-to-time-domain conversion usually induced by the frozen turbulence hypothesis, comparisons are made between covariance functions of intensity as well as averaged power.

Author Contact: Nicolas.perlot@dlr.de
Nicolas Perlot, Institute of Communications and Navigation,
German Aerospace Center (DLR), Site Oberpfaffenhofen, D-82234 Wessling, Germany

1.2. Background

In direct-detection receivers the received optical power P is the intensity I integrated over the Rx-aperture which can be a lens or a telescope primary mirror:

$$P = \int I(\boldsymbol{\rho}) W(\boldsymbol{\rho}) d\boldsymbol{\rho} \tag{1}$$

where $\boldsymbol{\rho}$ is a 2-dimensional vector in the aperture plane and W is the window aperture function defined by

$$W(\boldsymbol{\rho}) = \begin{cases} a, & \text{if} \quad \boldsymbol{\rho} \in A \\ 0, & \text{if} \quad \boldsymbol{\rho} \notin A \end{cases} \tag{2}$$

a is a constant and A is the aperture surface. Rigorously a equals one, but because we want to consider mean-normalized intensity as well as mean-normalized collected power, we set a = 1/area(A). Assuming a homogeneous (spatially stationary) intensity field in the receiver plane, we note $B_I(\boldsymbol{\rho})$ the intensity spatial covariance function. The covariance function of the collected power is given by [1]:

$$B_P(\boldsymbol{\rho}) = B_I(\boldsymbol{\rho}) * H_W(\boldsymbol{\rho}) \tag{3}$$

where * denotes convolution and

$$H_W(\boldsymbol{\rho}) = W(-\boldsymbol{\rho}) * W(\boldsymbol{\rho}) \tag{4}$$

is the optical transfer function of the aperture [2].
The normalized variance σ_P^2 of the received power (also called scintillation index of the irradiance flux) is thus given by:

$$\sigma_P^2 = B_P(0) = \int B_I(\boldsymbol{\rho}) H_W(-\boldsymbol{\rho}) d\boldsymbol{\rho} \tag{5}$$

We see that $B_I(\boldsymbol{\rho})$ turns out to be an important statistical measure regarding aperture averaging since it enables to derive the variance of the received power for any collecting aperture. If, in addition to statistical homogeneity, we assume statistical isotropy and an aperture with circular symmetry, the above functions can be expressed in terms of $\rho = |\boldsymbol{\rho}|$ only**.** Under those conditions, and introducing the polar coordinates r and θ, (3) can be rewritten as

$$B_P(\rho) = 2\int_0^{\pi} \int_0^{+\infty} B_I(r) H_W\left(\sqrt{r^2 + \rho^2 - 2\rho r \cos(\theta)}\right) r dr d\theta \tag{6}$$

In the common case of a circular lens aperture with diameter D, (4) can be rewritten as

$$H_W(\rho) = \left(\frac{4}{\pi D^2}\right)^2 K_0(\rho, D) \tag{7}$$

where the function $K_0(\rho,D)$ is defined by [3]

$$K_0(\rho,D)=\begin{cases}\dfrac{D^2}{2}\left[\cos^{-1}\left(\dfrac{\rho}{D}\right)-\left(\dfrac{\rho}{D}\right)\sqrt{1-\left(\dfrac{\rho}{D}\right)^2}\right], & \text{if } \rho\le D\\ 0, & \text{if } \rho>D\end{cases} \tag{8}$$

2. DESCRIPTION OF MEASUREMENTS AND HARDWARE SET-UP

2.1. Experimental scenario

The transmitter is a 810 nm laser emitting a beam with a divergence angle large enough to consider the wave spherical. The length of the path is L = 2.9 km. The link is located about 10 m above a rather flat ground. The C_n^2 parameter was evaluated according to the empirical formula [4]:

$$\begin{aligned}C_n^2 &= 3.8\times10^{-14}W + 2\times10^{-15}T - 2.8\times10^{-15}(RH) + 2.9\times10^{-17}(RH)^2\\ &\quad -1.1\times10^{-19}(RH)^3 - 2.5\times10^{-15}(WS) + 1.2\times10^{-15}(WS)^2\\ &\quad -8.5\times10^{-17}(WS)^3 - 5.3\times10^{-13}\end{aligned} \tag{9}$$

where the different parameters have been measured and have been set to:

W = 0.22; temporal hour weight
T = 284 K; air temperature
RH = 0.4; relative humidity
WS = 1.5 m/s; mean wind speed

We find $C_n^2 = 5.4\times10^{-14}$ $m^{-2/3}$. Formula (9) is meant to be valid up to a height of 15 m, so no further correction from height dependence is required. The inner and outer scale can be roughly estimated from the path height (≈ 10 m) [5] : l_0 = 5mm, L_0 = 5m.

An atmospheric phenomenon that is not considered here is global intermittency, the slow variations in space and time of the turbulence. Frehlich showed that global intermittency had minor effects on scintillation if the path length is larger than a few hundred meters [6]. Thus, hereafter, we will hold to our mean turbulence parameters to characterize the turbulent path. The corresponding Rytov index (a measure of the turbulence-integrated path for a plane wave [5]) is 13.2. Strong fluctuations are then expected.

At the receiver side, pupil images of a large lens are recorded on a CCD camera. The optical system is depicted in Fig. 1. A spherical lens with 130 mm diameter and 330 mm focal length has been used as objective of the optical system. Actually only an inner disc of 110 mm diameter will be considered in order to avoid too high spherical aberrations. An achromatic collimating lens of 5 mm focal length images the entrance pupil on a 2.1 mm × 2.1 mm CCD chip. The camera used is the DALSA CA-D1 featuring a frame transfer architecture, a 128×128 pixel resolution, a 100% fill factor and 8 data bits.

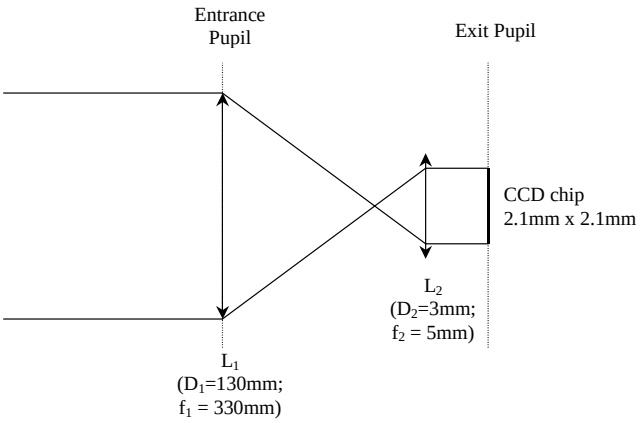

Fig. 1. Optical system for pupil recording

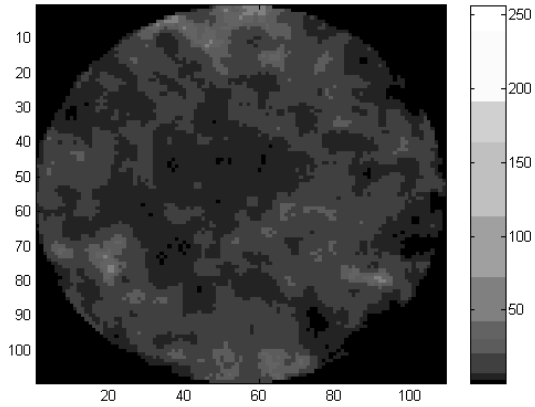

Fig. 2. Example of CCD frame with pupil image

The pixel sampling interval represents 1 mm in the entrance pupil, which is less than the inner scale l_0. Therefore, we can reasonably state that no spatial averaging occurs over one pixel and that images of intensity are recorded. Furthermore, in order to investigate spatial correlation, the size of the speckles must be small compared to the image extent. The Fresnel length of our scenario is

$$\sqrt{L/k} = 19.3 \text{ mm}$$

with k the wave number and L the path length. Under strong fluctuations, the correlation length of the received intensity is expected to be smaller than the Fresnel length. This means the extent of our recorded image is about at least 5 times larger than the correlation length.

To avoid temporal averaging during the CCD integration time, the intensity correlation time must be several times longer than the sampling time. For the experiment, the frame rate was set to 720 fps. Such a frame rate should cover the temporal spectrum of most scenarios with relatively weak wind (< 3 m/s). The mean wind speed during the experiment was measured at about 1.5 m/s. The duration of the recorded sequence is 45 s. Fig. 2 gives an example of a recorded pupil image.

2.2. Assessment of the measurement method

In order to compare the experimental results with the ensemble averages derived in theory, several assumptions are required. The assumption of spatial and temporal ergodicity for the scintillation process allows us to estimate the intensity PDF by counting the values of all the pixels present in the image sequence. As it is usually done in the fluctuation theory, stationarity in time and space of the optical field over the pupil surface will also be assumed.

Regarding the choice of a scenario, a CCD camera can be used for the recording of scintillation only under restricted conditions. The wind must not be too strong otherwise the limited frame rate of low-noise cameras cannot follow the fluctuations and time averaging occurs over the CCD integration time. If the entrance pupil is too large, a pixel may not represent a point aperture anymore, but already an averaged power. If the entrance pupil is smaller than the mean intensity speckle size, aperture averaging cannot be investigated. This upper bound set on the intensity correlation length eliminates all long-path scenarios (more than about 10 km) that remain in the weak-fluctuation regime. Finally, because the dynamic of the CCD camera is limited to the digital-number (DN) range [0..255], the quantization process may severely distort any statistical evaluation. Saturation of the intensity at 255 DN corrupts the scintillation index (SI) estimation. On the other hand, the lack of resolution for intensity values near zero makes difficult the modelling of the PDF and the estimation of the fade probabilities. As a measure of quantization distortion, the error on the SI has been evaluated for various intensity conditions (different mean and SI). Results are shown in Fig. 3 as a function of the intensity mean $\langle I \rangle$ in DN. A lognormal PDF has been assumed as initial intensity distribution and 3 SI values (0.8, 1.4 and 2) have been considered. The error introduced on the mean can be in most cases neglected, e.g., the mean error is

about 2% for SI = 2 and <*I*> = 30 DN. Distortions are most likely for scenarios lying in the focusing regime where the intensity variance is maximum.

Apart from these drawbacks, a big advantage of such measurements is that spatial and temporal behavior can be observed. One can see for example that, in the presence of significant transverse wind and short distances (L<1km), speckles can be observed moving across the 11 cm pupil while changing in shape only a little. This behavior can be directly related to the "frozen turbulence" phenomenon. An attempt to check the influence of the frozen turbulence hypothesis on the spatio-temporal process is made in section 4. Another advantage of the experimental setup is that aperture averaging effects can be easily investigated by means of pixel integration: this is how we estimate PDFs and temporal statistics for various aperture shapes.

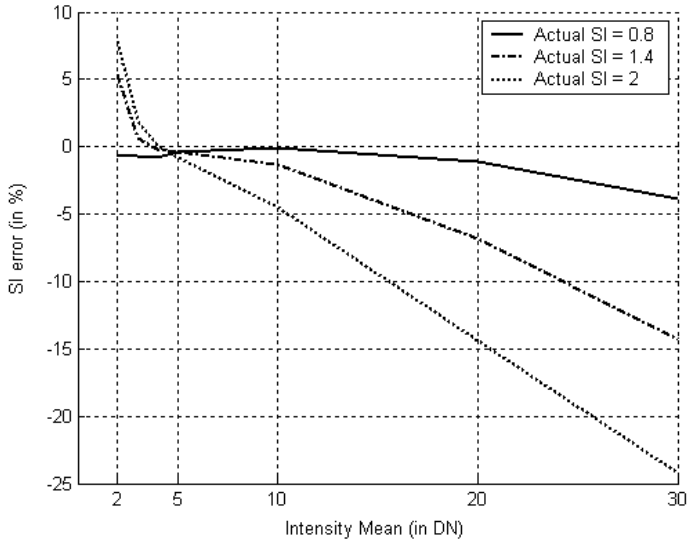

Fig. 3. Effects of the 0 to 255 DN CCD quantization on the scintillation index. The error on the scintillation index is given as a function of the mean and for different SI values (lognormal PDF assumed).

3. POWER PDF

3.1. Theory

Under the weak-fluctuation regime, the PDF of the averaged power can be approximated as lognormal. To the authors' knowledge, the analytical expression for the PDF of the sum of correlated lognormal variables is not available, and thus the error introduced by the lognormal approximation for the averaged power is not well defined. However numerical evaluations show that the lognormal shape is well conserved for low scintillation indices (i.e., $\sigma_I^2 < 0.3$). If very low scintillation is experienced, the lognormal PDF can further be approximated by a Gaussian PDF. This comes from the linearity of the exponential transformation in the vicinity of zero. One can reasonably assume a Gaussian PDF for power scintillation indices less than 0.01.

For the focusing and strong-fluctuation regimes, the lognormal PDF is generally valid neither for the intensity nor for the averaged power. In the extreme case of a scenario far in the saturation regime with an averaging consisting of the sum of two independent RVs, the PDF of the received power is given by the convolution of two exponential PDFs, namely $f_P(P) = e^{-P} * e^{-P} = Pe^{-P}$ with $P > 0$. Unlike for the case of weak fluctuations, the averaged power PDF conserves here a slope at the origin leading to enhanced deep fades.

3.2. Experimental power PDF from CCD pixel integration

By numerically integrating pixels over a given area of the captured images, we simulate the aperture averaging that occurs for direct-detection receivers.

Fig. 4 shows the experimental distribution of the averaged power for different circular apertures. The PDF for a point receiver corresponds to the counting of each pixel value of the pupil. For clarity, all averaged powers have been normalized to the pixel mean 20.4 DN. As pointed out in section 2, some pixel values may suffer from saturation at 255 DN. And this distortion will also affect the shape of the derived power PDFs. The derivation of the SI from the experimental intensity PDF gives $\sigma^2_{I,\mathrm{exp}}$ = 1.54. Assuming a lognormal distribution the SI without distortion would be about 15% higher. The error introduced by this distortion in the further analysis of the recorded data should be viewed as a primary source of uncertainty.

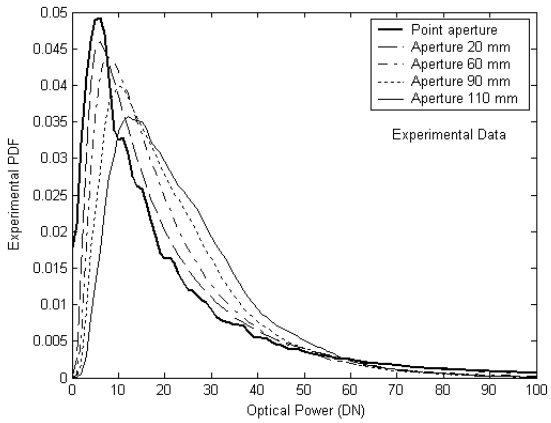

Fig. 4. Experimental PDFs.

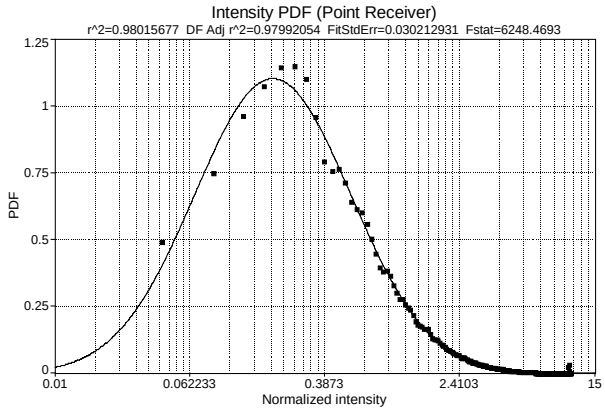

Fig. 5. Lognormal fit of the intensity distribution.

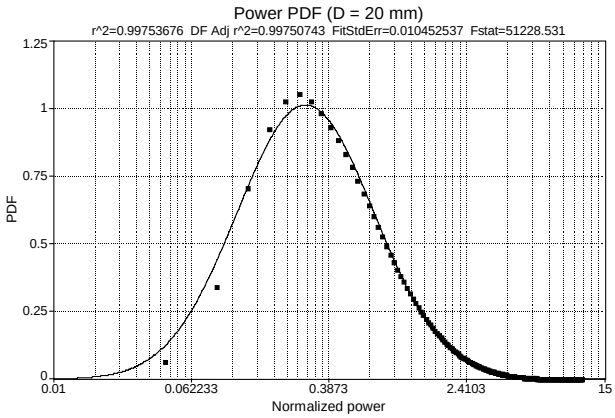

Fig. 6. Lognormal fit for the power averaged over a 20 mm aperture.

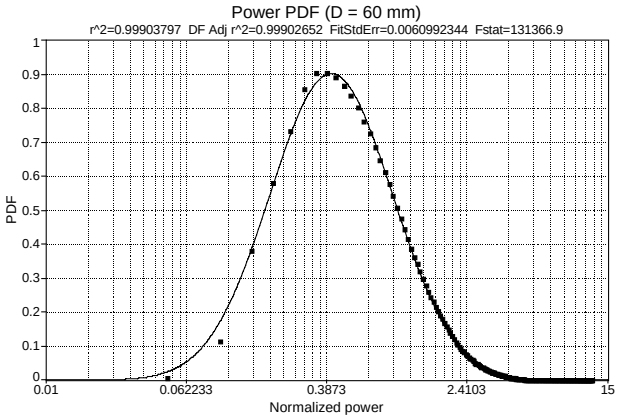

Fig. 7. Same as Fig. 6 for D = 60 mm.

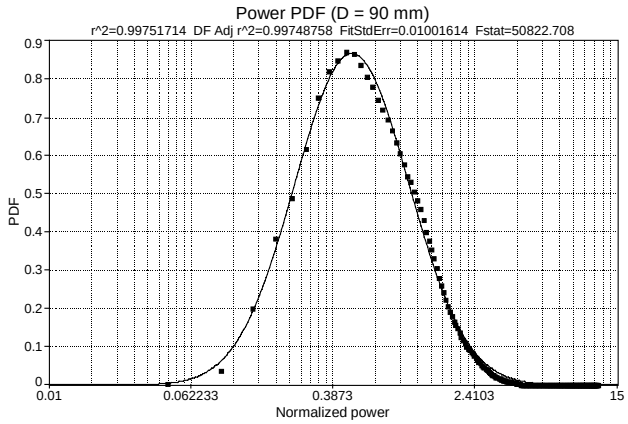

Fig. 8. Same as Fig. 6 for D = 90 mm.

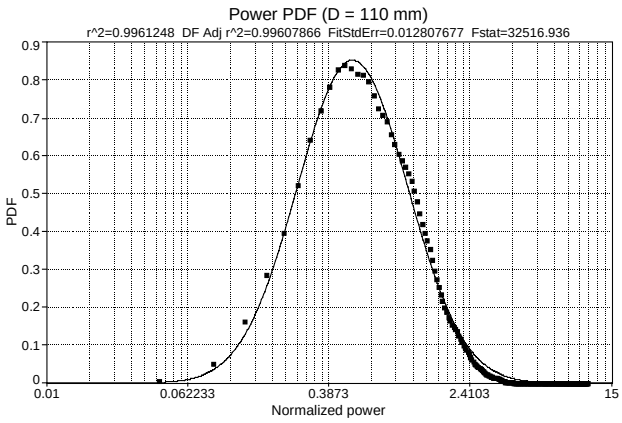

Fig. 9. Same as Fig. 6 for D = 110 mm.

A lognormal fit has been applied to each PDF curve displayed in Fig. 4. In the fitting process, every sample had the same weight and the mean power was normalized to one. The results are shown in Fig. 5 to 9 with a logarithmic scale for the x-axis. Above each modeled curve, four common goodness-of-fit statistics are given: the coefficient of determination "r^2", the coefficient of determination adjusted to the degree of freedom "Adj r^2", the fit standard error "FitStdErr" and the F-statistic "Fstat". As a fit becomes more ideal, the r^2 values approach 1.0, the standard error decreases toward zero, and the F-statistic goes toward infinity. The fit here corresponds to an optimization of r^2.

As it could have been expected under strong fluctuations, the intensity PDF (Fig. 5) departs more from the lognormal model as the averaged power PDFs (Fig. 6-9). This could have been expected knowing that the lognormal PDF is suited for weak fluctuations. The best lognormal fit has been observed here for D = 60 mm (Fig. 7).

3.3. Aperture averaging factor

Andrews et al. developed a method to predict quantitavely the reduction of scintillation through aperture averaging [5]. This method is based on an ABCD ray matrix formulation of the optical system with one Gaussian lens and enables the computation of the aperture averaging factor A_{SI}. The aperture averaging factor measures the reduction of the scintillation index relative to a point aperture:

$$A_{SI} = \frac{\sigma_P^2(D)}{\sigma_I^2} \tag{10}$$

Formulas presented in [5] leading to the aperture averaging factor, and valid under focusing and strong-fluctuation regimes, have been evaluated for the case of a spherical wave with the following link parameters: L = 2.9 km, l_0 = 5mm, L_0 = 5m and $C_n^2 = 5.4\times10^{-14}$ $m^{-2/3}$. In addition to the C_n^2 value derived from measurements (see § 2.1.), A_{SI} has been calculated for two other surrounding C_n^2 values to account for the uncertainty of the C_n^2 parameter. The corresponding theoretical A_{SI} curves are drawn in Fig. 10 along with the experimental estimates. Estimates of σ_P^2(D) were computed as the mean squares of the averaged power values normalized by their square means. Fig. 10 shows that theoretical curves tend to slightly underestimate the experimental A_{SI}. Underestimation had also been noted from Churnside's reported measurements for small apertures [5][7].

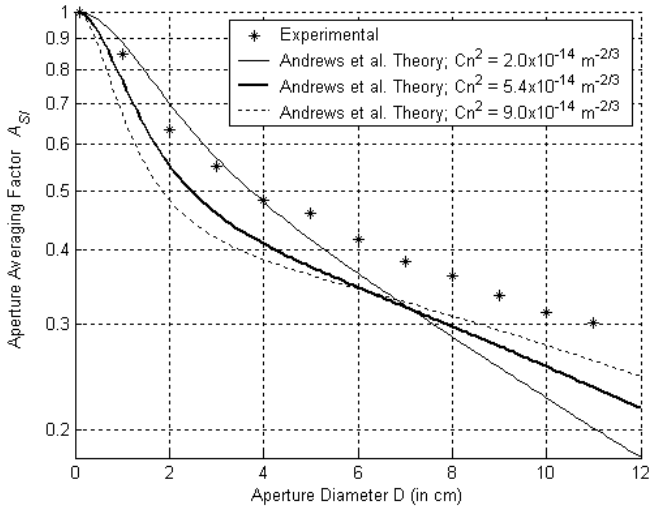

Fig. 10. Experimental and theoretical aperture averaging factors A_{SI}.

4. COVARIANCE FUNCTIONS AND FROZEN TURBULENCE HYPOTHESIS

4.1. Estimation of intensity covariance functions

Temporal correlation is usually deduced in theory from spatial correlation by introducing the mean transversal wind speed. However, if the transverse wind component is not significant enough then the applied conversion may give unrealistic temporal statistics.

Fig. 11 shows on the same graph experimental estimates of the temporal and spatial covariance functions. The functions are normalized so that their values at the origin are one. The curves have been scaled on their x-axes so that the correlation time τ_c and the correlation length ρ_c (both defined by the 1/e-crossing point) coincide. ρ_c and τ_c were found to be 0.014 m and 0.0082 s, respectively. The wind speed and direction were measured at the receiver. Wind data are listed in Table 1.

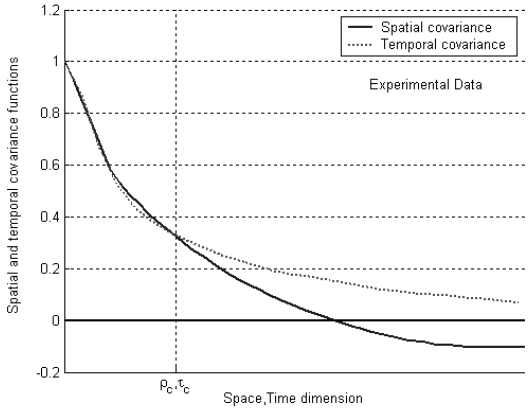

Fig. 11. Comparison of experimental spatial and temporal intensity covariance functions.

Wind speed (m/s)	Wind direction relative to beam direction
1.4	53°
1.6	99°
1.6	69°
1.6	68°
1.2	68°
0.5	66°
0.6	96°
0.8	115°
0.8	105°

Table 1. Wind data measured near receiver during the sequence recording. Wind data were evaluated every 5 s over a period of 45 s.

The temporal covariance function estimate was computed as follows. Considering the time series of a single pixel, we obtain a one-dimensional vector of 32400 samples and the unbiased cross-covariance sequence of the vector is calculated. To improve the estimation, the procedure is repeated for 4 other pixels randomly distributed over the pupil image in the CCD frame. The resulting cross-covariance sequences are then averaged.

As for the spatial covariance function, an estimate is calculated from each frame. The unbiased 2D-autocovariance function of each pupil image is worked out and then averaged over its polar angle coordinate [0, 2π] to obtain a 1D-autocovariance function. The distinct 32400 covariance estimates are then averaged.

It can be seen that both curves agree quite well for $\rho < \rho_c$ and $\tau < \tau_c$. For ρ and τ values larger than the 1/e-crossing points, the curves part and values of the spatial function become more questionable. Indeed, because of the final extent of recorded intensity image, the variance of the covariance estimate increases with ρ. The pupil diameter is only about 7 times bigger than ρ_c and the introduced uncertainty can explain the covariance departure for large ρ.

4.2. Temporal covariance functions of averaged power

Experimental estimates of the temporal covariance function $B_{P,\tau}(\tau)$ of the averaged power are displayed in Fig. 12 for various circular apertures. Again, the drawn curves represent average of covariance estimates calculated from different time series of integrated pixels.

A practical way of theoretically deriving the temporal covariance function of the averaged power is to make use of the frozen turbulence hypothesis and to multiply the argument of the spatial counterpart function by the mean transverse wind. The idea here is to check this spatial/temporal equivalence for the averaged power. First we convert the temporal intensity covariance function $B_{I,\tau}(\tau)$ to the spatial one $B_{I,\rho}(V\tau)$, where V is the mean transverse wind. By means of equation (6) to (8), the covariance function $B_{P,\rho}(\rho)$ of the power *P* averaged over a lens of diameter D is calculated. Then $B_{P,\rho}(\rho)$ is again converted to the temporal domain, leading to $B_{P,\tau}(\rho/V)$. It has been preferred to take as initial function the temporal intensity covariance function rather than the spatial one because $B_{I,\tau}(\tau)$ could be much more accurately estimated than its spatial counterpart $B_{I,\rho}(\rho)$.

Fig. 13 to 15 present the resulting $B_{P,\tau}(\tau)$ functions for 3 different mean wind speeds (V = 1, 1.5 and 2 m/s). Taking a high wind speed amounts to considering large intensity speckles that are swept across the pupil plane, thus leading to less aperture-averaging effect. As it can be seen, the power scintillation indices (variance values at $\tau = 0$ s) could not fit the experimental ones of Fig. 12. We see that in this attempt to use the equivalence of spatial and temporal statistics, no satisfactory results could be reached.

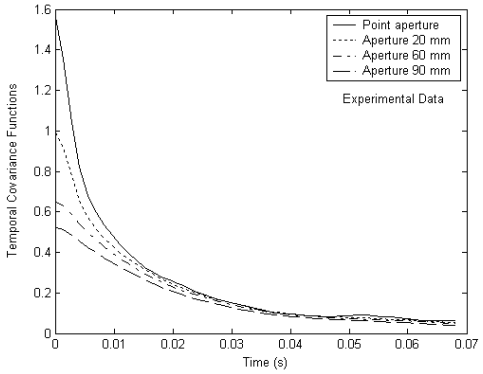

Fig. 12. Estimation of $B_P(\tau)$ from measurement data.

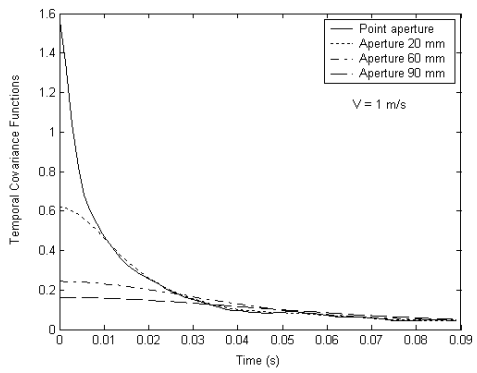

Fig. 13. Generated temporal covariance functions assuming equivalence with spatial covariance functions of averaged power. V = 1 m/s

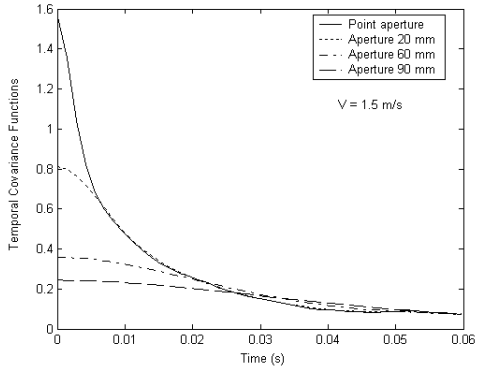

Fig. 14. Same as Fig. 13 for V = 1.5 m/s

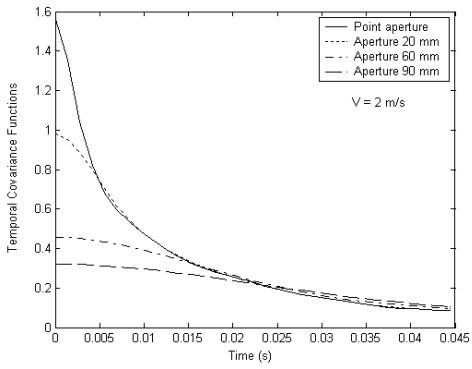

Fig. 15. Same as Fig. 13 for V = 2 m/s

5. CONCLUSIONS

A CCD-based instrument has been set up to investigate the aperture averaging of scintillation. In order to obtain a satisfactory recording of the pupil plane on a CCD camera, one must care for several aspects of the experimental scenario. The presented scenario could meet on the whole the different requirements and was besides well suited for the hypothesis of frozen turbulence. Intensity fluctuations and aperture averaging factor predicted by theory agreed fairly with the experimental data. Although a high correlation was found between temporal and spatial intensity covariance functions, the extension of this space/time equivalence for the second-order statistics of the aperture-averaged power failed markedly.

Similar measurements of scintillation in the saturation regime are planned using a logarithmic CMOS image sensor. The inherent higher dynamic range and frame rate of such sensors should lead to less distortion of the measured scintillation.

REFERENCES

1. A. Belmonte, A. Comerón, J. Bará, J. A. Rubio, "Averaging of Collected-Power Fluctuations by a Multiaperture Receiver System", *Optical Engineering*, Vol. 35, 10, Oct. 1996, pp 2773-2778.

2. R. Gagliardi, S. Karp: *Optical Communications*, John Wiley & Sons, New York, 1995.

3. D.L. Fried, Aperture averaging of scintillation; *JOSA*, 57 (1967) 169-175.

4. N. S. Kopeika, *A System Engineering Approach to Imaging*, SPIE Press, Bellingham (WA), 1998.

5. L.C. Andrews, R.L.Phillips, C. Y. Hopen, *Laser Beam Scintillation with Applications*, SPIE Press, Bellingham (WA), USA, 2001.

6. R. Frehlich, 1994: Effects of Global Intermittency on Laser Propagation in the Atmosphere, *Appl. Opt.*, Vol. 33, 5764-5769.

7. J. H. Churnside, Aperture averaging of optical scintillations in the turbulent atmosphere, *Appl. Opt.*, Vol. 30, 1982-1994, 1982.